BIOCHEMISTRY
including biophysical chemistry & molecular biology
Article

Biochemistry **2010,** *49,* 1477–1485 1477
DOI: 10.1021/bi902166d

New Insight into the Mechanism of Action of the Temporin Antimicrobial Peptides

Maria Rosaria Saviello,[‡] Stefania Malfi,[‡] Pietro Campiglia,[§] Andrea Cavalli,[∥,⊥] Paolo Grieco,[‡] Ettore Novellino,[‡] and Alfonso Carotenuto*[,‡]

[‡]*Department of Pharmaceutical and Toxicological Chemistry, University of Naples "Federico II", I-80131 Naples, Italy,* [§]*Department of Pharmaceutical Science, University of Salerno, I-84084 Fisciano, Salerno, Italy,* [∥]*Department of Pharmaceutical Science, University of Bologna, I-40126 Bologna, Italy, and* [⊥]*Department of Drug Discovery and Development, Italian Institute of Technology, I-16163 Genova, Italy*

Received December 17, 2009; Revised Manuscript Received January 18, 2010

ABSTRACT: Temporins constitute a family of amphipathic α-helical antimicrobial peptides (AMPs) and contain some of the shortest cytotoxic peptides, comprised of only 10−14 residues. We have recently investigated two members of this family, temporin A (TA) and temporin L (TL), because of their different spectra of antimicrobial activity and toxicity. Consequently, we developed new analogues with promising biological activities named Pro^3-TL and Gln^3-TA. In this work, we performed a detailed NMR analysis of the new analogues in SDS and DPC micelles, which mimic bacterial and mammalian membranes, respectively. NMR studies reveal that strongly hemolytic Gln^3-TA was in a stable helical conformation along the entire sequence, while weakly hemolytic but antimicrobial Pro^3-TL showed conformational averaging at the N-terminus. Furthermore, molecular dynamics (MD) simulations on TL and Pro^3-TL were performed in explicit water and DPC micelles. Simulations indicated that both peptides prefer a location at the micelle−water interface; however, Phe^1 of strongly hemolytic TL was embedded more in depth into DPC, and only TL caused a significant distortion of the micelle shape. By combining NMR and computational analyses, we obtained a molecular-level resolution of the interactions between TL and its analogues with membrane mimicking micelles.

Antimicrobial peptides (AMPs)[1] are considered key components of the innate immunity, which is found throughout the living world (*1*−*3*). A large variety of these molecules have been isolated from a vast array of biological sources, either prokaryotic or eukaryotic organisms, including humans, which they protect from the invasion of bacteria, protozoa, fungi, and viruses (*2*, *4*, *5*). AMPs display an extreme diversity in their primary and secondary structures and usually have a rather large spectrum of antibiotic activity. Low selectivity and fast killing of microbes are crucial features of this peptide-based defense mechanism and make it an "instant" immune system against microbial invaders (*6*−*8*). Importantly, AMPs are active against pathogens resistant to traditional antibiotics and thus offer the possibility of developing a new class of antibiotics (*2*, *9*−*11*).

Amphibian skin represents an incredibly rich source of AMPs, which are stored in granules of the dermal glands and secreted upon stress or contact with microorganisms (*3*, *12*). Among amphibian AMPs, temporins make up a family of related molecules, first isolated from the skin of the European red frog *Rana temporaria* (*13*). Many other members of this group, totaling now more than 70 peptides, were later found in several other *Rana* species and also in the venom of wasps (*14*−*17*). Structurally, temporins are characterized by being short peptides (10−14 residues) with a net positive charge at the neutral pH level and a potential to adopt an amphipathic α-helix structure upon contact with membranes or in hydrophobic environments. Temporins have been found to be active particularly against Gram-positive bacteria, *Candida* species, and fungi and to have the ability to bind and permeate both artificial and biological membranes (*12*, *18*−*21*). It is widely accepted that the main target of AMPs is the lipid bilayer of the bacterial membrane instead of specific membrane protein receptors (*22*). It is supposed that differences in lipid composition between bacterial and mammalian cell membranes are the main reasons for the selectivity of AMPs toward microbial cells (*22*, *23*). However, numerous AMPs can also bind and permeate the membranes of mammalian cells. Any attempt to design a peptide or peptidomimetic for therapeutic use would then be aided by a clear understanding of the structural elements that are responsible for its interaction with both mammalian and bacterial cell membranes. This would help in the engineering of new peptide sequences with similar/better antimicrobial activities but with a lower toxicity, provided that these properties are distinct and separable in the primary structure of the peptide. The lipid composition of bacterial membranes is quite different from that of eukaryotic cells. Bacterial membranes include substantial amounts of negatively charged phospholipids such as phosphatidylglycerol and

*To whom correspondence should be addressed: Department of Pharmaceutical and Toxicological Chemistry, University of Naples "Federico II", Via D. Montesano, 49, 80131 Napoli, Italy. Phone: +39-081-678626. Fax: +39-081-678630. E-mail: alfonso.carotenuto@unina.it.

[1]Abbreviations: AMPs, antimicrobial peptides; SDS, sodium dodecyl sulfate; DPC, dodecylphosphocholine; NMR, nuclear magnetic resonance; DQF-COSY, double-quantum-filtered correlated spectroscopy; TOCSY, total correlated spectroscopy; NOESY, nuclear Overhauser enhancement spectroscopy; NOE, nuclear Overhauser effect; MD, molecular dynamics; EM, energy minimization; 1D, 2D, and 3D, one-, two-, and three-dimensional, respectively; TSP, 3-(trimethylsilanyl)-propionic acid; PC, phosphatidylcholine. Abbreviations used for amino acids and designation of peptides follow the rules of the IUPAC-IUB Commission of Biochemical Nomenclature. Amino acid symbols denote the L-configuration unless indicated otherwise.

Published on Web 01/18/2010

Table 1: Peptide Sequences

peptide	sequence
TA	H-Phe^1-Leu^2-Pro^3-Leu^4-Ile^5-Gly^6-Arg^7-Val^8-Leu^9-Ser^{10}-Gly^{11}-Ile^{12}-Leu^{13}-NH_2
TL	H-Phe^1-Val^2-Gln^3-Trp^4-Phe^5-Ser^6-Lys^7-Phe^8-Leu^9-Gly^{10}-Arg^{11}-Ile^{12}-Leu^{13}-NH_2
Gln^3-TA	H-Phe^1-Leu^2-Gln^3-Leu^4-Ile^5-Gly^6-Arg^7-Val^8-Leu^9-Ser^{10}-Gly^{11}-Ile^{12}-Leu^{13}-NH_2
Pro^3-TL	H-Phe^1-Val^2-Pro^3-Trp^4-Phe^5-Ser^6-Lys^7-Phe^8-Leu^9-Gly^{10}-Arg^{11}-Ile^{12}-Leu^{13}-NH_2

cardiolipin (*24*). In contrast, the membrane of eukaryotic cells is composed mainly of phosphatidylcholine (PC), sphingomyelin, and cholesterol, all of which are neutrally charged at physiological pH (*25*).

In a previous work, we investigated two members of this family, temporin A (TA) and temporin L (TL) (Table 1) [temporins TA and TL are now also named 1Ta and 1Tl, respectively, according to the new nomenclature proposed by Conlon (*26*)], by spectroscopic and computational methods in membrane mimetic environments (SDS and DPC micelles), because of their different spectra of antimicrobial activity and toxicity (*27*). Briefly, TA is preferentially active against Gram-positive bacteria (*14*, *19*) and displays a low lytic activity against human erythrocytes (*19*). TL has a strong activity against both Gram-positive and Gram-negative bacteria but also shows high lytic activity against human erythrocytes (*18*, *28*). On the basis of NMR results for TA and TL, we hypothesized a different molecular mechanism underlying the antimicrobial and hemolytic activities of temporins. In particular, the "dynamic peptide-lipid supramolecular pore" (*20*) and the "barrel-stave" (*29*) models were employed to interpret the antimicrobial and hemolytic activities of temporins, respectively.

In this work, we performed a detailed NMR analysis of the new analogues, Pro^3-TL and Gln^3-TA, and compared their conformational behavior with that of the parent peptides, TA and TL, respectively. NMR analysis was performed in SDS and DPC micelles, which mimic bacterial and mammalian membranes, respectively (*30*). Since a drastic reduction in the hemolytic activity of Pro^3-TL compared to that of the parent TL was one of the major results of the previous investigation (*27*), molecular dynamics (MD) simulations were performed with TL and Pro^3-TL in explicit water and dodecylphosphocholine (DPC) micelles, to provide a possible explanation for the molecular mechanism underlying hemolytic activity.

MATERIALS AND METHODS

Material for Spectroscopic Studies. Samples of 99.9% ^2H_2O were obtained from Aldrich (Milwaukee, WI), and 98% SDS-d_{25} and DPC-d_{38} were obtained from Cambridge Isotope Laboratories, Inc. (Andover, MA). [2,2,3,3-Tetradeuterio-3-(trimethylsilanyl)]propionic acid (TSP) was from MSD Isotopes (Montreal, QC). 16-Doxylstearic acids were from Sigma, and $MnCl_2$ was from Merck (Darmstadt, Germany).

NMR Spectroscopy. Peptides were previously synthesized and tested (*27*). We prepared the samples for NMR spectroscopy by dissolving the appropriate amount of peptide in 0.55 mL of ^1H_2O or 0.05 mL of ^2H_2O to produce a concentration of 1−2 mM peptides and 200 mM SDS-d_{25} or DPC-d_{38}, respectively. The NMR experiments were performed at varying pH values. The samples were adjusted near the desired pH value using HCl and NaOH solutions. NH exchange studies were performed by dissolving peptides in 0.60 mL of ^2H_2O and 200 mM SDS-d_{25} or DPC-d_{38}. NMR spectra were recorded on a Varian Unity INOVA 700 MHz spectrometer equipped with a *z*-gradient 5 mm triple-resonance probe head. All the spectra were recorded at a temperature of 298.1 K. The spectra were calibrated relative to TSP (0.00 ppm) as an internal standard. One-dimensional (1D) NMR spectra were recorded in the Fourier mode with quadrature detection. 2D DQF-COSY (*31*, *32*), TOCSY (*33*), and NOESY (*34*) spectra were recorded in the phase-sensitive mode using the method from States (*35*). Data block sizes were 2048 addresses in t_2 and 512 equidistant t_1 values. A mixing time of 70 ms was used for the TOCSY experiments. NOESY experiments were conducted with mixing times in the range of 150−300 ms. The water signal was suppressed by gradient echo (*36*). The 2D NMR spectra were processed using the NMRPipe package (*37*). Before Fourier transformation, the time domain data matrices were multiplied by shifted $\sin^2$ functions in both dimensions, and the free induction decay size was doubled in F_1 and F_2 by zero filling. The qualitative and quantitative analysis of DQF-COSY, TOCSY, and NOESY spectra was conducted using the interactive program package XEASY (*38*). The temperature coefficients of the amide proton chemical shifts were calculated from 1D ^{1}H NMR and 2D TOCSY experiments performed at different temperatures in the range of 298−320 K by means of linear regression.

Spin-Label Experiments. We prepared the NMR samples by dissolving 2 mM peptides in 200 mM deuterated DPC solutions in a 90:10 H_2O/D_2O mixture. Assuming a micelle aggregation number of ~60, this corresponds to a micelle concentration of 3.3 mM. The 16-doxylstearic acids (solubilized in DMSO-d_6) and Mn^{2+} (dissolved in H_2O) were added to the samples at a concentration of one spin-label per micelle.

Structural Determinations. The NOE-based distance restraints were obtained from NOESY spectra recorded with a mixing time of 200 ms. The NOE cross-peaks were integrated with XEASY and were converted into upper distance bounds using CALIBA incorporated into DYANA (*39*). Only NOE-derived constraints were considered in the annealing procedures. An error tolerant target function (tf type 3) was used to account for the peptide intrinsic flexibility. For each examined peptide, an ensemble of 200 structures was generated with the simulated annealing of DYANA. Then 100 of 200 structures whose interproton distances best fitted NOE-derived distances were chosen and refined through successive steps of restrained and unrestrained EM calculations using the Discover algorithm (Accelrys, San Diego, CA) and the consistent valence force field (CVFF) (*40*). The minimization lowered the total energy of the structures; no residue was found in the disallowed region of the Ramachandran plot. The final structures were analyzed using InsightII (Accelrys). Graphical representations were conducted with InsightII. The root-mean-square deviation analysis between energy-minimized structures was conducted with MOLMOL (*41*). PROMOTIF was used to extract details about the location and types of structural secondary motifs (*42*).

Molecular Dynamics (MD) Simulations. The structure of a micelle, consisting of 65 molecules [Tieleman laboratory Web site (http://moose.bio.ucalgary.ca)], was used as the initial state of the micelle system. The initial conformation of the peptides was set to an α-helix as determined by NMR for TL in DPC (*27*). Furthermore, the helix was placed perpendicularly to the micelle surface as shown by paramagnetic probe investigations on TL in DPC (*27*). The micelle center of mass was overlapped with the center of mass of the peptide. The peptide insertion required five DPC monomers to be deleted. Amber 9 (*43*) was used for all minimizations and simulations of the solvated peptide/DPC micelle systems. The peptide parameters were defined by the parm99 force field (*44*), whereas the DPC molecules were parametrized by using Antechamber (*45*) with the General Amber Force Field (GAFF) (*45*). The TIP3P model was used for water molecules (*46*). The peptide/micelle/water complex was set in a rectangular-shaped box with the buffering distance set to 8 Å. Counterions were placed by the Leap module to neutralize the charges of the systems. As a first step, water molecule geometries were minimized. Then, to remove possible negative contacts between the peptides and the micelle, the entire system was minimized by 20000 steps of steepest descent followed by 10000 steps of conjugate gradient. After minimization, the systems were heated to 300 K by a weak coupling algorithm and were equilibrated for 185 ps. Then, 40 ns of MD simulations was conducted for each system under periodic boundary conditions. The cutoff was set to 10 Å. The long-range electrostatic interactions were calculated by means of the particle-mesh Ewald algorithm (*47*). The time step of the MD simulations was set to 1.5 fs, and the SHAKE algorithm was used to constrain hydrogen bond lengths at their equilibrium values. No atoms were kept fixed during the MD runs. The system pressure was maintained at 1 atm (NPT ensemble), and coordinates were saved for analysis every 0.15 ps.

RESULTS

NMR Analysis. A whole set of 1D and 2D NMR spectra were collected for Gln^3-TA and Pro^3-TL. Spectra were obtained from aqueous solutions of both SDS and DPC (T = 298.1 K). Complete ^{1}H NMR chemical shift assignments were effectively achieved for all the analyzed peptides according to the Wüthrich procedure (*48*) via the usual systematic application of DQF-COSY (*31*, *32*), TOCSY (*31*, *32*), and NOESY (*34*) experiments with the support of XEASY (Tables S1−S4 of the Supporting Information) (*38*). $^3J_{HN-H\alpha}$ couplings were difficult to measure probably because of a combination of smaller coupling constants (α-helical structure) and broader lines.

Gln^3-TA in SDS Solution. Diagnostic NMR parameters observed for Gln^3-TA in SDS solution, H_α chemical shifts, NOE contacts, NH exchange rates, and temperature coefficients (Supporting Information), all indicated a conformational propensity for helical structure. In particular, evidence of α-helix formation was provided by the analysis of the H_α resonances, which are strongly dependent on local secondary structure (*49*, *50*). Upfield shifts for H_α relative to random coil values are generally found for residues implicated in an α-helix or in turns and downfield shifts for those in β-sheets. H_α atoms from residue 2 to residue 13 experienced upfield shifts of the NMR signals compared to those observed for the same amino acids in the random coil state (Figure S1 of the Supporting Information). Additionally, a continuous stretch of NOE contacts of the types $d_{\alpha\beta(i,i+3)}$, $d_{\alpha\beta(i,i+4)}$, and $d_{NN(i,i+2)}$ could be observed along residues 3−12 (Figure S2a of the Supporting Information). All these data indicated the presence of an α-helix along the entire sequence of the peptide. NH temperature coefficients ($-\Delta\delta/\Delta T$ > 3.0 ppb/K) observed for residues 6, 8, 10, 12, and 13 indicated that such helical conformation was in equilibrium with more disordered conformations. Furthermore, the simultaneous presence of $d_{\alpha N(i,i+2)}$ NOEs along the entire sequence indicated the presence of β-turns in equilibrium with α-helix structure.

NMR-derived constraints obtained for Gln^3-TA in SDS were used as the input data for a simulated annealing structure calculation as implemented within the standard protocol of DYANA (*39*). NOE-derived constraints were translated into interproton distances and used as upper limit constraints in subsequent annealing procedures to produce 200 conformations from which 100 structures were chosen, whose interproton distances best fitted NOE-derived distances, and then refined through subsequent steps of restrained and unrestrained EM calculations using Discover (Accelrys). An ensemble of 50 structures satisfying the NMR-derived constraints (violations smaller than 0.50 Å) was chosen for further analysis. As shown in Figure 1a, Gln^3-TA exhibited an α-helix structure encompassing residues 4−10 (rmsd = 0.5 Å for the backbone heavy atoms of these residues). The side chain orientation was also well-defined (rmsd = 1.2 Å for the heavy atoms of residues 4−10). N- and C-terminal regions were less defined with the coexistence of folded and extended structures.

Gln^3-TA in DPC Solution. Gln^3-TA in DPC solution exhibited spectral features resembling those found in SDS solution. The differences between the NMR data in the two environments pointed to a higher conformational stability of Gln^3-TA in DPC micelles. In particular, we observed a larger number of medium-range NOE connectivities (Figure S2b of the Supporting Information), longer NH exchange times, and lower temperature coefficients for almost all residues, indicating that these NH groups were engaged in stronger hydrogen bonds, stabilizing the helical structure (Table S2 of the Supporting Information). Furthermore, H_α chemical shift values (Figure S1 of the Supporting Information) were significantly upfield-shifted in DPC solution compared to SDS solution. The shift was mainly observed for residues 1 and 2, which strongly indicated that the helical structure extended itself to the N-terminal residues in DPC solution. Another spectral feature indicating the structure stabilization of the N-terminal portion of Gln^3-TA in DPC was an intense downfield shift observed for the Leu^2 NH resonance (from 8.37 ppm in SDS to 9.36 ppm in DPC).

NMR-derived constraints obtained for Gln^3-TA in DPC were used as the input data for a simulated annealing structure calculation as described above. For each peptide, 50 calculated structures satisfying the NMR-derived constraints (violations smaller than 0.35 Å) were chosen. As shown in Figure 1b, Gln^3-TA exhibited an α-helix structure encompassing residues 2−13 (rmsd = 0.25 Å for the backbone heavy atoms), with some conformational averaging only in the N- and C-terminal regions. The side chain orientation was also well-defined (rmsd = 0.9 Å for all the heavy atoms).

Pro^3-TL in SDS Solution. Diagnostic NMR parameters observed for Pro^3-TL in SDS solution indicated a conformational propensity toward helical structure. H_α atoms from residue 2 to residue 13 experienced an upfield shift of the NMR signals compared to those observed for the same amino acids in the random coil state (Figure S1 of the Supporting Information). Analysis of the exchange rates and of the temperature coefficients

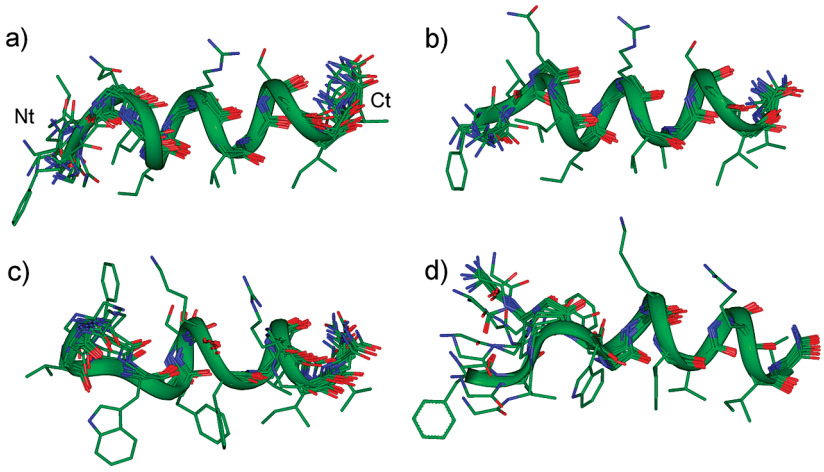

FIGURE 1: Superposition of the 20 lowest-energy conformers of Gln^3-TA in SDS (a), Gln^3-TA in DPC (b), Pro^3-TL in SDS (c), and Pro^3-TL in DPC (d). Structures were superimposed using the backbone heavy atoms of residues 3−11. Heavy atoms are shown with different colors (carbon, green; nitrogen, blue; oxygen, red). Hydrogen atoms are not shown for the sake of clarity. Only side chains of the lowest-energy conformer are shown for the sake of clarity. Backbone atoms of the lowest-energy conformer were evidenced as a ribbon. Nt, N-terminus; Ct, C-terminus.

Table 2: Remaining Amplitudes of NH−H_α TOCSY Cross-Peaks of Pro^3-TL in 200 mM DPC after Addition of Paramagnetic Probes[a]

probe	Val^2	Trp^4	Phe^5	Ser^6	Lys^7	Phe^8	Leu^9	Gly^{10}	Arg^{11}	Ile^{12}	Leu^{13}
16-doxyl	ov	0.6	ov	0.7	1.0	0.9	0.6	0.7	0.9	0.8	0.7
Mn^{2+}	ov	0.2	ov	0.2	0.3	0.4	0.3	0.2	0.2	0.2	0.04

[a]ov, overlapped signals.

for the NH resonance indicated that such a helical conformation was stable along residues 5−13, since NH resonances of these residues showed temperature coefficients ($-\Delta\delta/\Delta T < 3.0$ ppb/K) and exchange rates compatible with stable helical structures (Table S3 of the Supporting Information). The presence of $d_{\alpha N(i,i+2)}$, between Val^2 and Trp^4, indicated the presence of a β-turn in the N-terminal fragment of the peptide. Structure calculation gave an ensemble of 50 structures satisfying the NMR-derived constraints (violations smaller than 0.60 Å). Many structures (41 of 50) of Pro^3-TL showed an α-helix along residues 6−11. A few conformers (9 of 50) showed the α-helix encompassing residues 4−12. Many structures (36 of 50) showed the N-terminal residues in turn conformations. β-Turns centered on Pro^3 and Leu^4 and inverse γ-turns centered on Pro^3 could be observed (Figure 1c).

Pro^3-TL in DPC Solution. Pro^3-TL in DPC solution showed spectral features resembling those found in SDS solution, with similar NOE connectivities (Figure S2d of the Supporting Information), NH exchange rates, NH temperature coefficients, and proton resonances (Table S4 of the Supporting Information). The largest differences between the NMR data in the two environments were observed in the N-terminal region of the peptide. In particular, H_α chemical shift values (Figure S1 of the Supporting Information) for residues Phe^1 and Leu^2 were significantly upfield-shifted in DPC solution compared to SDS solution. Subsequent structure calculations (see above) gave an ensemble of 50 structures satisfying the NMR-derived constraints (violations smaller than 0.50 Å). Almost all the structures (42 of 50) folded in an α-helix structure along residues 6−13, while some (8 of 50) showed a helix encompassing all residues (rmsd = 0.9 Å for the backbone heavy atoms). Many structures (42 of 50) showed β- and γ-turn structures about N-terminal residues (Figure 1d) as observed in SDS. Therefore, the structure of Pro^3-TL in DPC can be described as a β-turn at the N-terminus (residues 2−5) followed by an α-helix (residues 6−13). This helical region was more stable than the corresponding region of the other described systems (rmsd = 0.08 Å for the backbone heavy atoms vs 0.10 Å of Gln^3-TA in DPC).

Topological Orientation. The positioning of the peptide Pro^3-TL relative to the surface and interior of the DPC micelle was studied using paramagnetic probes: 16-doxylstearic acid and Mn^{2+}. Unpaired electrons led to dramatically accelerated longitudinal and transverse relaxation rates of protons in spatial proximity via highly efficient spin and electron relaxation. Therefore, these paramagnetic probes were expected to cause broadening of the NMR signals and a decrease in resonance intensities from residues outside the micelle (Mn^{2+}) or deeply buried in the micelle (16-doxyl) (*51*, *52*). TOCSY spectra of Pro^3-TL (in DPC solution) in the presence and absence of the spin-labels, with all other conditions kept constant, were recorded (Table 2). The signal intensities of N-terminal residues 4 and 6 showed significant reductions (~30−40%) after the addition of 16-doxylstearic acid. Upon the addition of Mn^{2+}, a generalized reduction of signal intensity was observed (>60% reduction), and more strongly for C-terminal 10−13 residues (>80% reduction). Therefore, Pro^3-TL is preferentially located at the liquid−water interface of the micelles. The reduction of the magnitudes of the signals of the N-terminal residues upon addition of 16-doxylstearic acid indicated that the N-terminal tail of the peptide can flip inward and outward from the micelle core.

pH Titration of TL and Pro^3-TL in DPC Solution. To investigate the charge state of the protonatable functions (N-terminus, Lys^7 amino group, and Arg^{11} guanidinium group) of the peptides in DPC solution, TOCSY spectra were recorded for TL and Pro^3-TL at different pH values. In particular, an upfield shift was observed for the H_α chemical shift of Phe^1 residue upon variation of the pH from 5 to 8 (Figure 2). The observed chemical shift changes of Phe^1 H_α were the result of the dynamic equilibrium between a charged and noncharged Phe^1 amino

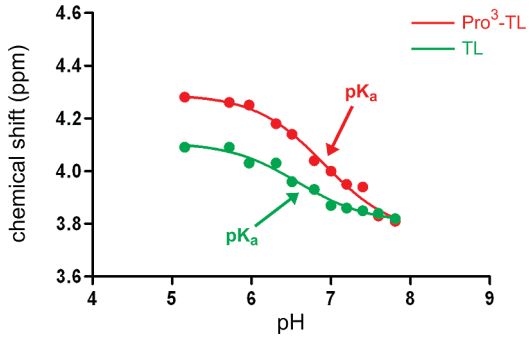

FIGURE 2: pH titration of TL and Pro^3-TL in DPC solution.

group. Following this chemical shift variation, we could determine an apparent pK_a value for the N-terminal amino group. These pK_a values are 6.6 and 7.0 for TL and Pro^3-TL, respectively. Hence, for both peptides, the Phe^1 amino group is in equilibrium between the charged and uncharged states at the blood pH value (7.4), with a prevalence (2.8-fold for Pro^3-TL and 6.5-fold for TL) of the uncharged state. The other protonatable groups did not change their positively charged state, since the variation of side chain proton resonances was negligible upon titration from pH 5 to 8 (data not shown).

Molecular Dynamics. MD simulations were performed for TL and Pro^3-TL in explicit water and DPC micelles. On the basis of titration data, both neutral (TL_N and Pro^3-TL_N) and positively charged (TL_C and Pro^3-TL_C) N-termini were taken into account.

Conformational Behavior. Considering the peptide conformational behavior, TL (both TL_N and TL_C) maintained a dominant helical conformation throughout the entire simulations while Pro^3-TL (both states) lost the helical conformation at the N-terminal segment, in agreement with NMR data (Tables S5−S8 of the Supporting Information).

Relative Peptide−Micelle Positions. Peptides diffused from the micelle's core to the interface region of the micelle during the 40 ns simulation, in all systems. We argued this by plotting the distances between the center of mass (CM) of the peptides and the CM of the micelle (Figure 3) or between the N-terminal nitrogen atom of the peptide and the CM of the micelle (Figure 4) over the simulation time.

However, while the N-termini of TL_C and Pro^3-TL_C rapidly moved to the surface, the N-terminus of Pro^3-TL_N remained within the micelle for a significantly longer period of time (~13 ns), and the N-terminus of TL_N oscillated during most of the simulation period. Finally, the N-termini of Pro^3-TL_N and TL_N were quite embedded into DPC (N-terminus−micelle distance of ~15 Å) compared to the charged N-termini (N-terminus−micelle distance of ~20 Å) (Figure 4).

Peptide−Micelle Interactions. Both TL and Pro^3-TL diffused from the micelle's core to the interface region of the micelle during the 40 ns simulations. The best location we could identify by means of MD simulations was that with hydrophobic residues embedded into lipids and hydrophilic residues in water (Figure 5). To provide a quantitative estimation of the interactions between the peptide and micelle, we calculated both hydration numbers and radial distribution functions (RDFs).

Hydration number was defined as the number of water molecules within 3 Å of a predefined residue. It provided the number of water molecules located near the residue, allowing us to identify those residues in water (high hydration numbers) and

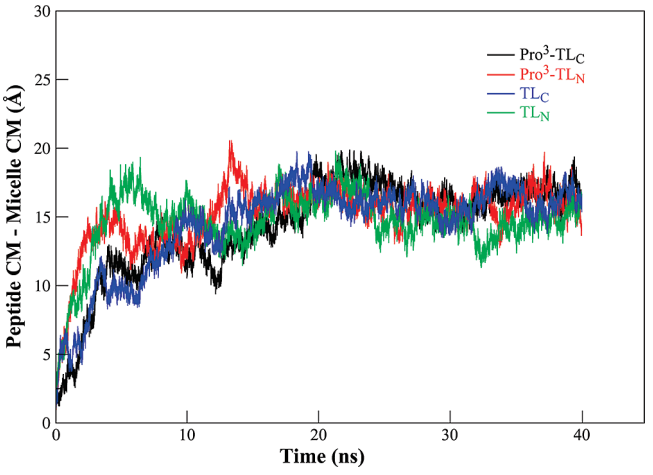

FIGURE 3: Distances between the CM of the peptides and the CM of the micelle.

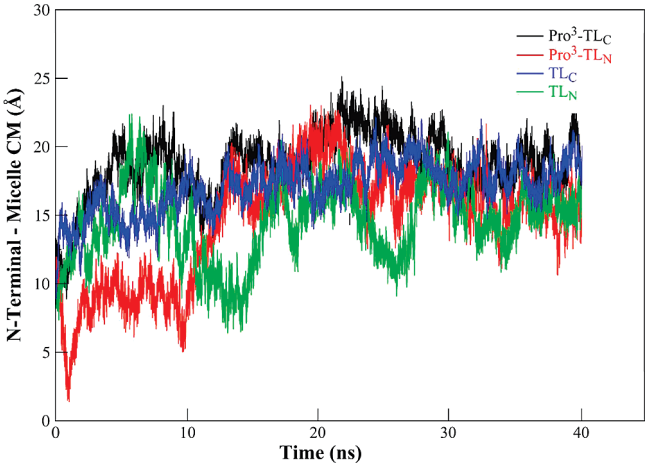

FIGURE 4: Distances between the N-terminal nitrogen atom of the peptide and the CM of the micelle.

those embedded in the micelle (low hydration numbers). Two sets of hydration numbers were calculated for each system, one for the side chain atoms and the other for the backbone carbonyl carbons (Table 3). The C-terminus was usually more hydrated than the N-terminus as demonstrated by the carbonyl carbon hydration numbers. As far as side chains were concerned, the least hydrated residues were Val^2, Phe^5, Leu^9, and Ile^{12} in all systems. Besides these, the Phe^1 side chain of TL_N exhibited a very low hydration number. This was in good agreement with the position of the N-terminus of TL_N in the interior of the DPC micelle. Conversely, the most hydrated side chains were the Trp^4, Ser^6, Lys^7, and Arg^{11} residues for all systems. Interestingly, Gln^3 exhibited the highest hydration number for both TL_N and TL_C.

Radial distribution functions (RDFs) describe the distribution of surrounding atoms as a function of the distance from a predefined atom. RDFs between the side chain atoms and the negatively charged group on the micelle heads were calculated. The four systems showed similar RDFs for each residue when the phosphate headgroups were taken into account. As expected, arginines showed somewhat stronger interactions with DPC phosphate groups compared to other hydrophilic residues (Figures S3−S6 of the Supporting Information).

Influence of the Peptide on Micelle Shape. The effect of each peptide on DPC micelle shape can be quantified by comparing some properties of the micelle (see below) in the

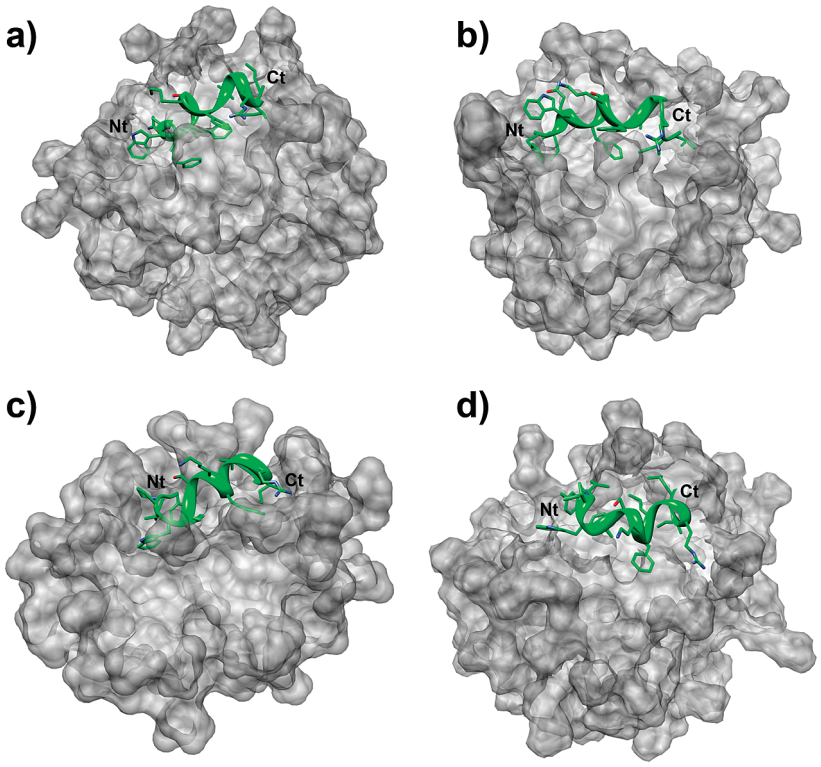

FIGURE 5: Snapshots illustrating the final (40 ns) location of TL_N (a), TL_C (b), Pro^3-TL_N (c), and Pro^3-TL_C (d) in DPC micelles (gray). Peptides are similarly oriented with the N-terminus (Nt) to the left and the C-terminus (Ct) to the right.

Table 3: Hydration Numbers[a]

	carbonyl carbons				side chains			
	TL_C	TL_N	Pro^3-TL_C	Pro^3-TL_N	TL_C	TL_N	Pro^3-TL_C	Pro^3-TL_N
Phe^1	0.097	0.020	0.12	0.72	0.36	0.060	0.63	0.43
Val^2	0.0020	0.46	0.05	0.036	0.025	0.19	0.14	0.14
Gln^3/Pro^3	0.56	0.93	0.58	0.84	3.2	3.3	0.27	0.32
Trp^4	0.23	0.20	0.44	0.72	1.61	1.5	1.8	1.3
Phe^5	0.0060	0.0020	0.030	0.044	0.040	0.050	0.01	0.023
Ser^6	0.84	0.67	0.35	0.74	1.5	1.6	1.2	1.4
Lys^7	1.0	0.86	0.60	0.74	3.1	3.0	2.7	3.0
Phe^8	0.060	0.12	0.030	0.29	0.92	0.38	0.28	0.70
Leu^9	0.024	0.010	0.0050	0.078	0.11	0.090	0.010	0.13
Gly^{10}	0.75	0.74	0.65	0.82	–	–	–	–
Arg^{11}	0.67	0.73	0.65	0.84	2.6	2.5	2.6	2.5
Ile^{12}	0.51	0.67	0.49	0.65	0.060	0.030	0.040	0.090
Leu^{13}	0.96	0.99	0.73	1.1	0.18	0.23	0.14	0.23

[a]The hydration numbers are averaged over the 40 ns of each simulation and are calculated for a radius of hydration of 3.0 Å.

presence of the peptide to the same properties computed for the pure micelle. The stability of the micelles was checked using the ratio of three momenta of inertia and eccentricity, in addition to simple visual inspection of snapshots of the system. Three momenta of inertia (I_1, I_2, and I_3) were calculated along arbitrarily predefined orthogonal vectors. R_1 is the I_2/I_1 ratio, R_2 the I_3/I_1 ratio, and R_3 the I_1/I_1 ratio (obviously, $R_3 = 1$), where I_1 is the momentum of inertia along the x, y, or z axis with the smallest magnitude. For a perfect sphere, all these ratios are equal to 1. Tieleman argued that the micelles are not perfectly spherical systems and, for pure DPC micelles of 54 and 65 lipids, reported R_1, R_2, and R_3 values of 1.13, 1.08, and 1, and 1.19, 1.10, and 1, respectively (*53*). Here, we observed that the DPC micelle (60 lipids) was partially distorted by TL_N, while TL_C, Pro^3-TL_C, and Pro^3-TL_N did not greatly affect the micelle shape (Table 4).

Table 4: Average Momenta of Inertia, Their Ratios, and Eccentricities (e) of the DPC Micelles

	TL_N	TL_C	Pro^3-TL_N	Pro^3-TL_C
I_1 (amu/nm^2)	108114	99520.9	172735	111593
I_2 (amu/nm^2)	133692	116684	203242	128975
I_3 (amu/nm^2)	124896	111194	194489	125378
R_1	1.24	1.17	1.17	1.16
R_2	1.15	1.12	1.12	1.12
e	0.116	0.088	0.092	0.085

Another parameter used to define the micelle shape was eccentricity. It is defined as $e = 1 - I_1/I_{avg}$, where I_1 was defined as described above and I_{avg} is the average of three momenta of inertia. For a perfect sphere, this value should be equal to zero.

Tieleman found eccentricity values of 0.066 and 0.087 for pure DPC micelles of 54 and 65 lipids, respectively (*53*). Eccentricity values found in our systems (Table 4) again indicated that TL_N significantly affected the overall shape of the aggregated complex.

DISCUSSION

The aim of this study was to provide new insight into the mechanism of antimicrobial and hemolytic (toxic) action of the AMP temporins. Starting from two members of this family of AMPs (TL and TA), we have recently developed two analogues with promising biological activities named Pro^3-TL and Gln^3-TA (Table 1) (*27*). In particular, Pro^3-TL exhibited an increased antimicrobial activity toward Gram-positive and yeast cells, with a hemolytic activity 2−5-fold lower than that of the natural TL, over a concentration range of 3−12 μM. Gln^3-TA also exhibited promising antimicrobial activity, but its hemolytic activity became significantly stronger compared to that of parent peptide TA (up to 10-fold higher).

As the first step of this work, we studied the conformational properties of such temporin analogues by solution NMR. NMR analysis was performed in SDS and DPC micelles, which mimic bacterial and mammalian membranes, respectively (*30*). In fact, uni- or multilamellar phospholipid vesicles are not suitable for high-resolution NMR studies of membrane-associated peptides and proteins. Because overall vesicular reorientation rates are too low for high-resolution NMR, detergent micelles, usually composed of SDS or DPC, have served in the role of membrane mimetic since the early NMR structure determination of biopolymers (*54*, *55*). Indeed, micelles are commonly used in place of phospholipid monolayers or bilayers in methods such as NMR spectroscopy (*56*, *57*). Although there is no direct correlation between the structure of the SDS headgroup and that of phospholipids composing a bacterial membrane, the SDS micelle is generally considered to be a reliable model for bacterial membranes, since it possesses an anionic outer surface and a hydrophobic inner core (*58*, *59*). Similarly, DPC micelles are considered reliable models of eukaryotic cell membranes, which are generally rich in zwitterionic phospholipids (*60*). Solution NMR studies of amphibian AMPs, recently reviewed (*61*), were largely performed in micelle solutions. However, it is worth mentioning that the micelle-bound structures of membrane active peptides need to be further validated by comparative investigations with explicit lipid bilayers.

In both SDS and DPC solutions, the two analyzed peptides exhibited structures which could be described as amphipathic α-helices at least when considering central residues 6−10 (Figure 1). The helical character of Gln^3-TA significantly increased passing from SDS to DPC micelles. The whole peptide sequence was involved in this helical strengthening. This was particularly evident at the N-terminus of the peptide. In fact, residues Phe^1 and Leu^2 changed from a disordered state to a helical conformation (Figure 1). In Pro^3-TL, the N-terminal residues preferred turn conformations mostly centered on the Pro^3 residue. Such turn conformations were observed both in SDS and in DPC solutions.

The conformational behavior of Gln^3-TA and Pro^3-TL was in good agreement with the rational strategy originally exploited in designing such derivatives (*27*). In particular, since the hemolytic activity of TL was associated with its strong propensity for helical structure at the N-terminus, a proline residue was placed in position 3 with the aim of inducing a turn structure in the derivative Pro^3-TL. Conversely, replacement of the native proline residue with a glutamine in TA should lead to increased helical content at the N-terminus. Here, we experimentally determined the existence of N-terminal turn structures in the weakly hemolytic Pro^3-TL, and α-helix in the same region of Gln^3-TA. This confirms that helical content controls the hemolytic effect, while it is irrelevant to the antimicrobial activity of the temporins. Thus, the "carpetlike" or the "dynamic peptide-lipid supramolecular pore" models, which do not need any particular peptide conformation, can hold in explaining temporin's antimicrobial activity (*27*).

Since a drastic reduction in the hemolytic activity of Pro^3-TL compared to that of the parent TL was one of the major results of our investigations, MD simulations were performed for TL and Pro^3-TL in explicit water and DPC micelles, providing a mechanistic view underlying the hemolytic activity. To provide a more realistic comparison between simulations and experiments, we conducted MD runs in micelles. MD simulations were performed on peptides having both neutral (TL_N and Pro^3-TL_N) and positively charged (TL_C and Pro^3-TL_C) N-terminal functions. The two states are both populated at blood pH (7.4) as indicated by pH titration (Figure 2). The simulation results confirmed the experimental conformational tendencies observed by the NMR study with TL in an α-helical conformation throughout the entire simulations, with Pro^3-TL (both states) showing a flexible N-terminal segment (Tables S5−S8 of the Supporting Information).

Both TL and Pro^3-TL diffused from the micelle's core to the interface region of the micelle (Figures 3 and 4). Hydrophobic residues were embedded in lipids, while hydrophilic residues were solvent-exposed (Figure 5). Hydrophilic residues seem to be endowed with different roles in the peptide−micelle interaction. Calculating RDFs (Figures S3−S6 of the Supporting Information), we could determine that the Arg^{11} side chain mainly interacted with DPC phosphate groups, because of the very favorable electrostatic interaction between the protonated guanidinium group and the negatively charged phosphate; Ser^6, Lys^7, and Gln^3 (in TL) side chains mainly interacted with water molecules, as shown by the high hydration numbers (Table 3).

Some differences could be observed among the simulated systems. (a) Uncharged N-termini of TL_N and Pro^3-TL_N were embedded more in depth into the DPC than the charged N-termini. (b) TL_N showed a low hydration number at the side chains of the Phe^1 residue (Table 3). (c) Only TL_N caused a significant distortion of the micelle shape (Table 4). Considering that pH titration established a prevalence (6.5-fold) of the uncharged state at the N-terminus of TL and only of 2.8-fold for Pro^3-TL, these differences indicated that TL, mainly in its TL_N state, perturbed the DPC micelle surface in accordance with its high hemolytic effect.

Combined results of NMR and MD simulations could shed light on the molecular mechanism underlying the hemolytic activity of these derivatives. Recently, we have hypothesized the so-called barrel-stave (*29*) model to explain the hemolytic activity of TL and analogues (*27*). In this model, the peptides are supposed to form the staves of a barrel-like channel: the helical peptide should insert within the lipid bilayer placing itself almost perpendicular to the membrane surface. MD simulation results are apparently in contrast with the barrel-stave model, since all peptides localize at the micelle−water interface. In more detail, strongly hemolytic TL behaves as a rigid helical rod, with the N-terminal Phe^1 embedded in the hydrophobic lipid core and C-terminal residues more exposed to the water bulk. Therefore,

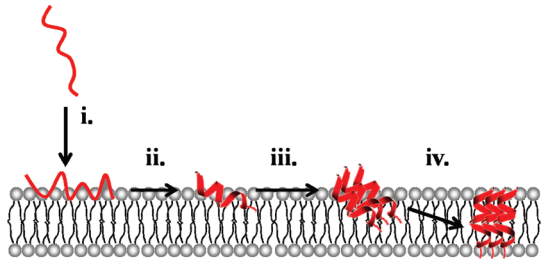

FIGURE 6: Schematic illustration of the stages in the membrane association−folding−aggregation pathway (adapted and modified from ref *64*). For the sake of clarity, the possible formation of tail-to-tail dimers is not depicted.

the location of TL was not perfectly parallel to the micelle surface, but it is somewhat tilted and can be seen as a "hoe ploughing the fields". Phe^1 and Phe^5 are the blades, and Arg^{11} is the handle anchored to the phosphate of the DPC. The resulting furrow on the micelle surface is filled with water molecules dragged by Gln^3, Ser^6, and Lys^7 side chains.

The lack of depth of insertion of TL into zwitterionic lipids is in contrast with experimental results obtained by us (*27*) and others (*21*, *62*). However, since TL undergoes a very rapid local aggregation after its application on vesicles surface (*21*), one can argue that the reorientation and membrane insertion steps can occur only after the oligomerization step. Hence, the following highly interconnected sequence of events can be speculatively proposed (Figure 6). (i) electrostatically enhanced initial association of a random coil peptide to the membrane surface, (ii) conformational change from a random coil to an amphipathic α-helix, with the peptide long axis almost parallel to the membrane layer plane, (iii) aggregation of the α-helical peptides into oligomers, and (iv) reorientation and membrane insertion of the peptide, its long axis becoming perpendicular to the monolayer surface.

Eventually, oligomers can organize in channel-like structures (barrel-stave model). In this model, the hydrophobic facet of the amphipathic helix seals with the hydrocarbon chain of the bilayer while the hydrophilic surface points inward, producing an aqueous pore. A peptide length of ~23 residues is required to span the membrane bilayer. Since TL is only a 13-mer peptide, a tail-to-tail dimerization was proposed to suit the barrel-stave model (*13*, *14*). Such a dimerization was experimentally observed for the 15-mer antibiotic peptide, gramicidin (*63*). Interestingly, neutral amino terminal groups, prevailing in TL, should favor the CN−NC dimerization avoiding charge repulsion. The processes described above may further evolve into the formation of nontoxic amyloid (*64*). Hence, while the carpetlike or the dynamic peptide-lipid supramolecular pore models could explain temporin's antimicrobial activity, the barrel-stave model could be employed to interpret their hemolytic effect. Noteworthy is the fact that melittin also uses the carpetlike mechanism for negatively charged membranes and the barrel-stave model for zwitterionic membranes (*65*).

In summary, by combining spectroscopic (NMR) and computational analyses we obtained a molecular-level resolution of the interactions between TL and its analogues with membrane mimicking micelles. The knowledge of the peptide conformational behavior and of the interaction mode of any single amino acid with the membrane models may aid in the design of new antimicrobial peptides with improved antimicrobial activity and a weakened hemolytic effect to combat antibiotic-resistant pathogens.

ACKNOWLEDGMENT

NMR spectral data were provided by Centro di Ricerca Interdipartimentale di Analisi Strumentale, Università degli Studi di Napoli "Federico II". The assistance of the staff is gratefully appreciated.

SUPPORTING INFORMATION AVAILABLE

Tables of chemical shifts, chemical shift deviations, NOE connectivities, dihedral angles during the MD runs, and RDFs. This material is available free of charge via the Internet at http://pubs.acs.org.

REFERENCES

1. Boman, H. G. (2000) Innate immunity and the normal microflora. *Immunol. Rev. 173*, 5–16.
2. Zasloff, M. (2002) Antimicrobial peptides of multicellular organisms. *Nature 415*, 389–395.
3. Mangoni, M. L., Miele, R., Renda, T. G., Barra, D., and Simmaco, M. (2001) The synthesis of antimicrobial peptides in the skin of *Rana esculenta* is stimulated by microorganisms. *FASEB J. 15*, 1431–1432.
4. Bulet, P., Stocklin, R., and Menin, L. (2004) Anti-microbial peptides: From invertebrates to vertebrates. *Immunol. Rev. 198*, 169–184.
5. Zaiou, M. (2007) Multifunctional antimicrobial peptides: Therapeutic targets in several human diseases. *J. Mol. Med. 85*, 317–329.
6. Boman, H. G. (1995) Peptide antibiotics and their role in innate immunity. *Annu. Rev. Immunol. 13*, 61–92.
7. Boman, H. G. (2003) Antibacterial peptides: Basic facts and emerging concepts. *J. Intern. Med. 254*, 197–215.
8. Kimbrell, D. A., and Beutler, B. (2001) The evolution and genetics of innate immunity. *Nat. Rev. Genet. 2*, 256–267.
9. Hancock, R. E. W. (2001) Cationic peptides: Effectors in innate immunity and novel antimicrobials. *Lancet Infect. Dis. 1*, 156–164.
10. Mookherjee, N., and Hancock, R. E. (2007) Cationic host defence peptides: Innate immune regulatory peptides as a novel approach for treating infections. *Cell. Mol. Life Sci. 64*, 922–933.
11. Papagianni, M. (2003) Ribosomally synthesized peptides with antimicrobial properties: Biosynthesis, structure, function, and applications. *Biotechnol. Adv. 21*, 465–499.
12. Rinaldi, A. C. (2002) Antimicrobial peptides from amphibian skin: An expanding scenario. *Curr. Opin. Chem. Biol. 6*, 799–804.
13. Simmaco, M., Mignogna, G., Canofeni, S., Miele, R., Mangoni, M. L., and Barra, D. (1996) Temporins, antimicrobial peptides from the European red frog *Rana temporaria*. *Eur. J. Biochem. 242*, 788–792.
14. Wade, D., Silberring, J., Soliymani, R., Heikkinen, S., Kilpeläinen, I., Lankinen, H., and Kuusela, P. (2007) Antibacterial activities of temporin A analogs. *FEBS Lett. 479*, 6–9.
15. Wade, D., Silveira, A., Silberring, J., Kuusela, P., and Lankinen, H. (2000) Antibiotic properties of novel synthetic temporin A analogs and a cecropin A-temporin A hybrid peptide. *Protein Pept. Lett. 7*, 349–357.
16. Wade, D. (2002) Unambiguous consensus sequences for temporin-like antibiotic peptides. *Int. J. Chem. 5*, 5.
17. Mangoni, M. L. (2006) Temporins, anti-infective peptides with expanding properties. *Cell. Mol. Life Sci. 63*, 1060–1069.
18. Rinaldi, A. C., Mangoni, M. L., Rufo, A., Luzi, C., Barra, D., Zhao, H., Kinnunen, P. K. J., Bozzi, A., Di Giulio, A., and Simmaco, M. (2002) Temporin L: Antimicrobial, hemolytic and cytotoxic activities, and effects on membrane permeabilization in lipid vesicles. *Biochem. J. 368*, 91–100.
19. Mangoni, M. L., Rinaldi, A. C., Di Giulio, A., Mignogna, G., Bozzi, A., Barra, D., and Simmaco, M. (2000) Structure-function relationships of temporins, small antimicrobial peptides from amphibian skin. *Eur. J. Biochem. 267*, 1447–1454.
20. Rinaldi, A. C., Di Giulio, A., Liberi, M., Gualtieri, G., Oratore, A., Schinina, M. E., Simmaco, M., and Bozzi, A. (2001) Effects of temporins on molecular dynamics and membrane permeabilization in lipid vesicles. *J. Pept. Res. 58*, 213–220.
21. Zhao, H., Rinaldi, A. C., Di Giulio, A., Simmaco, M., and Kinnunen, P. K. J. (2002) Interactions of the antimicrobial peptides temporins with model biomembranes. Comparison of temporins B and L. *Biochemistry 41*, 4425–4436.
22. Shai, Y. (1999) Mechanism of the binding, insertion and destabilization of phospholipid bilayer membranes by α-helical antimicrobial and cell non-selective membrane-lytic peptides. *Biochim. Biophys. Acta 1462*, 55–70.

23. Matsuzaki, K. (1999) Why and how are peptide-lipid interactions utilized for self-defense? Magainins and tachyplesins as archetypes. *Biochim. Biophys. Acta 1462*, 1–10.
24. Yang, L., Weiss, T. M., Lehrer, R. I., and Huang, H. W. (2000) Crystallization of antimicrobial pores in membranes: Magainin and protegrin. *Biophys. J. 79*, 2002–2009.
25. Gidalevitz, D., Ishitsuka, Y., Muresan, A. S., Konovalov, O., Waring, A. J., Lehrer, R. I., and Lee, K. Y. (2003) Interaction of antimicrobial peptide protegrin with biomembranes. *Proc. Natl. Acad. Sci. U.S.A. 100*, 6302–6307.
26. Conlon, J. M. (2008) Reflections on a systematic nomenclature for antimicrobial peptides from the skins of frogs of the family Ranidae. *Peptides 29*, 1815–1819.
27. Carotenuto, A., Malfi, S., Saviello, M. R., Campiglia, P., Gomez-Monterrey, I., Mangoni, M. L., Marcellini Hercolani Gaddi, L., Novellino, E., and Grieco, P. (2008) A different molecular mechanism underlying antimicrobial and hemolytic actions of Temporins A and L. *J. Med. Chem. 51*, 2354–2362.
28. Mangoni, M. L., Papo, N., Barra, D., Simmaco, M., Bozzi, A., Di Giulio, A., and Rinaldi, A. C. (2004) Effects of the antimicrobial peptide temporin L on cell morphology, membrane permeability and viability of *Escherichia coli*. *Biochem. J. 380*, 859–865.
29. Shai, Y. (1995) Molecular recognition between membrane-spanning polypeptides. *Trends Biochem. Sci. 20*, 460–464.
30. Langham, A. A., Khandelia, H., and Kaznessis, Y. N. (2006) How can a β-sheet peptide be both a potent antimicrobial and harmfully toxic? Molecular dynamics simulations of protegrin-1 in micelles. *Biopolymers 84*, 219–231.
31. Piantini, U., Sorensen, O. W., and Ernst, R. R. (1982) Multiple quantum filters for elucidating NMR coupling network. *J. Am. Chem. Soc. 104*, 6800–6801.
32. Marion, D., and Wüthrich, K. (1983) Application of phase sensitive two-dimensional correlated spectroscopy (COSY) for measurements of ^{1}H-^{1}H spin-spin coupling constants in proteins. *Biochem. Biophys. Res. Commun. 113*, 967–974.
33. Braunschweiler, L., and Ernst, R. R. (1983) Coherence transfer by isotropic mixing: Application to proton correlation spectroscopy. *J. Magn. Reson. 53*, 521–528.
34. Jenner, J., Meyer, B. H., Bachman, P., and Ernst, R. R. (1979) Investigation of exchange processes by two-dimensional NMR spectroscopy. *J. Chem. Phys. 71*, 4546–4553.
35. States, D. J., Haberkorn, R. A., and Ruben, D. J. A (1982) two-dimensional nuclear Overhauser experiment with pure absorption phase in four quadrants. *J. Magn. Reson. 48*, 286–292.
36. Hwang, T. L., and Shaka, A. J. (1995) Water suppression that works. Excitation sculpting using arbitrary wave-forms and pulsed-field gradients. *J. Magn. Reson. 112*, 275–279.
37. Delaglio, F., Grzesiek, S., Vuister, G. W., Zhu, G., Pfeifer, J., and Bax, A. (1995) NMRPipe: A multidimensional spectral processing system based on UNIX pipes. *J. Biomol. NMR 6*, 277–293.
38. Bartels, C., Xia, T., Billeter, M., Guentert, P., and Wüthrich, K. (1995) The program XEASY for computer-supported NMR spectral analysis of biological macromolecules. *J. Biomol. NMR 6*, 1–10.
39. Güntert, P., Mumenthaler, C., and Wüthrich, K. (1997) Torsion angle dynamics for NMR structure calculation with the new program DYANA. *J. Mol. Biol. 273*, 283–298.
40. Maple, J., Dinur, U., and Hagler, A. T. (1988) Derivation of force fields for molecular mechanics and dynamics from ab initio energy surface. *Proc. Natl. Acad. Sci. U.S.A. 85*, 5350–5354.
41. Koradi, R., Billeter, M., and Wüthrich, K. (1996) MOLMOL: A program for display and analysis of macromolecular structures. *J. Mol. Graphics 14*, 51–55.
42. Hutchinson, E. G., and Thornton, J. M. (1996) PROMOTIF: A program to identify and analyze structural motifs in proteins. *Protein Sci. 5*, 212–220.
43. Case, D. A., Darden, T. A., Cheatham, T. E., Simmerling, C. L., Wang, J., Duke, R. E., Luo, R., Merz, K. M., Pearlman, D. A., Crowley, M., Walker, R. C., Zhang, W., Wang, B., Hayik, S., Roitberg, A., Seabra, G., Wong, K. F., Paesani, F., Wu, X., Brozell, S., Tsui, V., Gohlke, H., Yang, L., and Tan, C. (2006) AMBER9, University of California, San Francisco.
44. Wang, J. M., Cieplak, P., and Kollman, P. A. (2000) How well does a restrained electrostatic potential (RESP) model perform in calculating conformational energies of organic and biological molecules? *J. Comput. Chem. 21*, 1049–1074.
45. Wang, J., Wang, W., Kollman, P. A., and Case, D. A. (2006) Automatic atom type and bond type perception in molecular mechanism calculations. *J. Mol. Graphics Modell. 25*, 247–260.
46. Jorgensen, W. L., Chandrasekhar, J., Madura, J. D., Impey, R. W., and Klein, M. L. (1983) Comparison of simple potential functions for simulating liquid water. *J. Chem. Phys. 79*, 926–935.
47. Zhou, R., Harder, E., Xu, H., and Berne, B. J. (2001) Efficient multiple time step method for use with Ewald and particle mesh Ewald for large biomolecular systems. *J. Chem. Phys. 115*, 2348–2358.
48. Wüthrich, K. (1986) in NMR of Proteins and Nucleic Acids, John Wiley & Sons, Inc., New York.
49. Wishart, D. S., Sykes, B. D., and Richards, F. M. (1992) The chemical shift index: A fast method for the assignment of protein secondary structure through NMR spectroscopy. *Biochemistry 31*, 1647–1651.
50. Andersen, N. H., Liu, Z., and Prickett, K. S. (1996) Efforts toward deriving the CD spectrum of a 3_{10} helix in aqueous medium. *FEBS Lett. 399*, 47–52.
51. Brown, L. R., Bösch, C., and Wüthrich, K. (1981) Location and orientation relative to the micelle surface for glucagon in mixed micelles with dodecylphosphocholine: EPR and NMR studies. *Biochim. Biophys. Acta 642*, 296–312.
52. Lindberg, M., Jarvet, J., Langel, U., and Graslund, A. (2001) Secondary structure and position of the cell-penetrating peptide transportan in SDS micelles as determined by NMR. *Biochemistry 40*, 3141–3149.
53. Tieleman, D. P., Van Der Spoel, D., and Berendsen, H. J. C. (2000) Molecular dynamics simulations of dodecylphosphocholine micelles at three different aggregate sizes: Micellar structure and chain relaxation. *J. Phys. Chem. B 104*, 6380–6388.
54. Brown, L. R., and Wüthrich, K. (1977) NMR and ESR studies of the interactions of cytochrome c with mixed cardiolipin phosphatidylcholine vesicles. *Biochim. Biophys. Acta 468*, 389–410.
55. Wüthrich, K., Bosch, C., and Brown, L. R. (1980) Conformational studies of lipid-bound polypeptides by elucidation of proton−proton cross-relaxation networks. *Biochem. Biophys. Res. Commun. 95*, 1504–1509.
56. Wang, G. (2008) NMR of membrane-associated peptides and proteins. *Curr. Protein Pept. Sci. 9*, 50–69.
57. Henry, G. D., and Sykes, B. D. (1994) Methods to study membrane protein structure in solution. *Methods Enzymol. 239*, 515–535.
58. Chandrababu, K. B., Ho, B., and Yang, D. (2009) Structure, dynamics, and activity of an all-cysteine mutated human β defensin-3 peptide analogue. *Biochemistry 48*, 6052–6061.
59. Lee, S. A., Kim, Y. K., Lim, S. S., Zhu, W. L., Ko, H., Shin, S. Y., Hahm, K. S., and Kim, Y. (2007) Solution structure and cell selectivity of piscidin1 and its analogues. *Biochemistry 46*, 3653–3663.
60. Saravanan, R., Bhunia, A., and Bhattacharjya, S. (2010) Micelle-bound structures and dynamics of the hinge deleted analog of melittin and its diastereomer: Implications in cell selective lysis by D-amino acid containing antimicrobial peptides. *Biochim. Biophys. Acta 1798*, 128–139.
61. Haney, E. F., Hunter, H. N., Matsuzaki, K., and Vogel, H. J. (2009) Solution NMR studies of amphibian antimicrobial peptides: Linking structure to function? *Biochim. Biophys. Acta 1788*, 1639–1655.
62. Zhao, H., and Kinnunen, P. K. (2002) Binding of the antimicrobial peptide temporin L to liposomes assessed by Trp fluorescence. *J. Biol. Chem. 277*, 25170–25177.
63. Kovacs, F., Quine, J., and Cross, T. A. (1996) Validation of the single-stranded channel conformation of gramicidin A by solid-state NMR. *Proc. Natl. Acad. Sci. U.S.A. 96*, 7910–7915.
64. Mahalka, A. K., and Kinnunen, P. K. (2009) Binding of amphipathic α-helical antimicrobial peptides to lipid membranes: Lessons from temporins B and L. *Biochim. Biophys. Acta 1788*, 1600–1609.
65. Papo, N., and Shai, Y. (2003) Exploring peptide membrane interaction using surface plasmon resonance: Differentiation between pore formation versus membrane disruption by lytic peptides. *Biochemistry 42*, 458–466.